

1 **Examination of Brown Carbon Absorption from Wildfires in the Western U.S. During the**  
2 **WE-CAN Study**

3  
4  
5 Amy P. Sullivan<sup>1</sup>, Rudra P. Pokhrel<sup>2,\*</sup>, Yingjie Shen<sup>2</sup>, Shane M. Murphy<sup>2</sup>, Darin W. Toohey<sup>3</sup>,  
6 Teresa Campos<sup>4</sup>, Jakob Lindaas<sup>1</sup>, Emily V. Fischer<sup>1</sup>, and Jeffrey L. Collett, Jr.<sup>1</sup>  
7

8  
9 <sup>1</sup>Colorado State University, Department of Atmospheric Science, Fort Collins, Colorado 80523

10 <sup>2</sup>University of Wyoming, Department of Atmospheric Science, Laramie, WY 82071

11 <sup>3</sup>University of Colorado – Boulder, Department of Atmospheric and Oceanic Sciences, Boulder,  
12 CO 80309

13 <sup>4</sup>National Center for Atmospheric Research, Atmospheric Chemistry Division, Boulder, CO

14 <sup>\*</sup>now at Cooperative Institute for Research in Environmental Sciences, University of Colorado,  
15 Boulder, CO 80309 and NOAA Chemical Science Laboratory, Boulder, CO 80305  
16

17 Corresponding author: Amy P. Sullivan, [sullivan@atmos.colostate.edu](mailto:sullivan@atmos.colostate.edu)  
18  
19  
20  
21  
22  
23  
24  
25  
26  
27  
28  
29  
30  
31  
32  
33  
34  
35  
36  
37  
38  
39  
40  
41  
42  
43  
44  
45  
46

47 **Abstract**

48 Light absorbing organic carbon, or brown carbon (BrC), can be a significant contributor  
49 to the visible light absorption budget. However, the sources of BrC and the contributions of BrC  
50 to light absorption are not well understood. Biomass burning is thought to be a major source of  
51 BrC. Therefore, as part of the WE-CAN (Western Wildfire Experiment for Cloud Chemistry,  
52 Aerosol Absorption and Nitrogen) Study BrC absorption data was collected aboard the  
53 NSF/NCAR C-130 aircraft as it intercepted smoke from wildfires in the Western U.S. in July-  
54 August 2018. BrC absorption measurements were obtained in near real-time using two  
55 techniques. The first coupled a Particle-into-Liquid Sampler (PILS) with a Liquid Waveguide  
56 Capillary Cell and a Total Organic Carbon analyzer for measurements of water-soluble BrC  
57 absorption and WSOC (water-soluble organic carbon). The second employed a custom-built  
58 Photoacoustic Aerosol Absorption Spectrometer (PAS) to measure total absorption at 405 and  
59 660 nm. The PAS BrC absorption at 405 nm (PAS total Abs 405 BrC) was calculated by  
60 assuming the absorption determined by the PAS at 660 nm was equivalent to the black carbon  
61 (BC) absorption and the BC aerosol absorption Ångström exponent was 1. Data from the PILS  
62 and PAS were combined to investigate the water-soluble vs. total BrC absorption at 405 nm in  
63 the various wildfire plumes sampled during WE-CAN. WSOC, PILS water-soluble Abs 405,  
64 and PAS total Abs 405 tracked each other in and out of the smoke plumes. BrC absorption was  
65 correlated with WSOC ( $R^2$  value for PAS = 0.42 and PILS = 0.60) and CO (carbon monoxide)  
66 ( $R^2$  value for PAS = 0.76 and PILS = 0.55) for all wildfires sampled. The PILS water-soluble  
67 Abs 405 was corrected for the non-water-soluble fraction of the aerosol using the calculated  
68 UHSAS (Ultra-High-Sensitivity Aerosol Spectrometer) aerosol mass. The corrected PILS water-  
69 soluble Abs 405 showed good closure with the PAS total Abs 405 BrC with a factor of ~1.5 to 2  
70 difference. This difference was explained by particle vs. bulk solution absorption measured by  
71 the PAS vs. PILS, respectively, and confirmed by Mie Theory calculations. During WE-CAN,  
72 ~45% (ranging from 31% to 65%) of the BrC absorption was observed to be due to water-soluble  
73 species. The ratio of BrC absorption to WSOC or  $\Delta$ CO showed no clear dependence on fire  
74 dynamics or the time since emission over 9 h.

75  
76  
77  
78  
79  
80  
81  
82  
83  
84  
85  
86  
87  
88  
89  
90  
91  
92

## 93 1. Introduction

94 Organic compounds can comprise a large fraction of PM (particulate matter) mass  
95 [Kanakidou *et al.*, 2005; Zhang *et al.*, 2007]. Organic carbon can be directly emitted or formed  
96 in the atmosphere from a variety of sources. This leads to organic aerosol particles composed of  
97 a number of compounds that range from insoluble to highly water-soluble and that can scatter or  
98 absorb light [Jacobson *et al.*, 2000; Saxena and Hildemann, 1996, and references therein].

99 The portion of organic carbon that is light-absorbing has been referred to as brown  
100 carbon (BrC) due to its yellow or brown color when concentrated, and it is likely to be a  
101 significant contributor to the visible light-absorption budget [Andreae and Gelencsér, 2006].  
102 Recent modeling studies have predicted a non-negligible effect on the Earth's radiation balance  
103 from BrC [Feng *et al.*, 2013; Zhang *et al.*, 2017; Zhang *et al.*, 2020]. Global measurements have  
104 shown that BrC can contribute up to 48% of the overall warming effect by absorbing  
105 carbonaceous aerosols [Zeng *et al.*, 2020]. BrC may also suppress photolysis rates of some  
106 chemical reactions, including decreasing surface ozone concentrations in certain locations, due to  
107 its ability to absorb at ultraviolet wavelengths [Jo *et al.*, 2016]. Some portion of BrC is likely  
108 composed of toxins, such as nitro- and oxy-aromatic species, suggesting BrC could also have  
109 health impacts [Desyaterik *et al.*, 2013; Verma *et al.*, 2015; Zhang *et al.*, 2013]. BrC itself is  
110 thought to have both primary and secondary sources. Particles from biomass burning or  
111 incomplete combustion of fossil fuels generally contain significant amounts of BrC (e.g.,  
112 [Chakrabarty *et al.*, 2010; Hoffer *et al.*, 2006; Kirchstetter *et al.*, 2004; Kirchstetter and  
113 Thatcher, 2012; Lack *et al.*, 2012; Lukács *et al.*, 2007]). Laboratory studies have observed  
114 production of BrC from a number of formation processes. This has included heterogeneous  
115 reactions of isoprene on acidic aerosol particles, a variety of aqueous-phase reactions, and  
116 reactions of organic compounds in acidic solutions (e.g., [Hoffer *et al.*, 2006; Limbeck *et al.*,  
117 2013; Sareen *et al.*, 2010; Updyke *et al.*, 2012]). However, there is still limited information on  
118 the contribution of BrC to total light absorption and the sources of BrC as there are few ambient  
119 measurements.

120 Total absorption measurements (black carbon (BC) + BrC) at multiple wavelengths can  
121 be used to determine BrC absorption due to the strong wavelength dependence of BrC. This  
122 requires the assumptions that: (1) the absorption Ångström exponent (AAE) for BC is known, (2)  
123 AAE is constant with wavelength, and (3) BrC does not absorb at longer wavelengths. The AAE  
124 for BC is well constrained at 1 in the visible and near-infrared wavelengths [Moosmüller *et al.*,  
125 2009]. The BrC absorption at other wavelengths is then found by difference from the  
126 extrapolated BC AAE [Lack and Langridge, 2013; Mohr *et al.*, 2013]. This approach can be  
127 applied to any technique that measures absorption at multiple wavelengths, including  
128 photoacoustic spectroscopy (PAS).

129 BrC can also be quantified by isolating the BrC chromophores by extraction of particles  
130 in solvents, such as water or methanol, in order to separate them from the insoluble BC and then  
131 measuring the light absorption of the soluble organic chromophores [Hecobian *et al.*, 2010].  
132 This is the only direct method to separate and quantify BrC as the light absorption from liquid  
133 extracts does not suffer from interferences by BC as they can be isolated by dissolution. A  
134 spectrophotometer with an UV/Vis (ultraviolet/visible) light source can provide high spectral  
135 resolution over a wide wavelength range from 200 to 800 nm. In addition, when coupled with a  
136 long-path liquid waveguide capillary absorption cell (LWCC), it also provides a highly sensitive  
137 measurement. This technique can be used off-line with filters or on-line with an aerosol

138 collection device such as Particle-into-Liquid Sampler (PILS) (e.g., [Hecobian *et al.*, 2010; Liu  
139 *et al.*, 2013, 2014, 2015; Zhang *et al.*, 2011, 2013].

140 Here we report BrC absorption data from a PAS and PILS-LWCC-TOC system to  
141 compare total vs. water-soluble BrC absorption in wildfire smoke. Data are from smoke plume  
142 penetrations during the Western Wildfire Experiment for Cloud Chemistry, Aerosol Absorption  
143 and Nitrogen (WE-CAN), an aircraft-based study focused on investigating the chemistry and  
144 transformation of emissions from wildfires in the western U.S. We examine the relationship  
145 between the BrC absorption and species known to be from biomass burning. We discuss how  
146 parameters such as aging and fire dynamics might influence BrC absorption from wildfires.  
147

## 148 2. Methods

### 149 2.1. The Airborne Mission

150 The WE-CAN Campaign was a multi-investigator study conducted aboard the National  
151 Science Foundation/National Center for Atmospheric Research (NSF/NCAR) C-130 aircraft.  
152 The C-130 was operated out of Boise, ID from Jul. 20 to Aug. 31, 2018. A suite of instruments  
153 was deployed for measurements of aerosol and trace gas composition. A total of 16 research  
154 flights sampled wildfire smoke over the western U.S. to characterize emissions, mixing,  
155 chemical transformations, and transport. Figure 1 presents a map of the flight transects and  
156 locations of the wildfires sampled. (We exclude Flight RF14, which was conducted off the coast  
157 of CA to sample a stratus deck impacted by smoke, and Flight RF16, which consisted of an  
158 intercomparison performed near Boise between WE-CAN and BB-FLUX (Biomass Burning  
159 Flux Measurements of Trace Gases and Aerosols) common measurements.) More information  
160 on each wildfire including the type of fuel consumed is available in the WE-CAN Field Catalog  
161 (catalog.eol.ucar.edu/we-can). WE-CAN sampled both fresh and aged (for Flights RF05 and  
162 RF08 along with parts of Flights RF07 and RF13) emissions from smoke for wildfires burning in  
163 CA, OR, WA, ID, MT, UT, and NV. The general sampling strategy was to circle the wildfire at  
164 the source and then follow the smoke downwind using a multiple transect search and rescue  
165 pattern to examine smoke evolution. Typically, wildfire smoke plumes were sampled in the free  
166 troposphere between 3-5 km during early afternoon to evening periods (20:00 to 02:00 UTC or  
167 14:00 to 20:00 LT). Flight RF08 and part of Flight RF07 were exceptions as the aircraft sampled  
168 the boundary layer (below 2 km) over the Central Valley of CA.  
169

### 170 2.2. Particle Collection

171 During WE-CAN, we deployed two Particle-into-Liquid Sampler (PILS) systems. A  
172 PILS is an aerosol collection device that continuously collects ambient particles into purified  
173 water [Orsini *et al.*, 2003]. After particles are grown inside the body of the PILS by water  
174 condensation in a supersaturated water vapor environment, formed through mixing the ambient  
175 air sample with saturated air (100% relative humidity) at higher temperature, the particles are  
176 collected by an impactor. The impactor plate is continually washed off by a flow of liquid  
177 passed over the impactor, providing a liquid sample containing dissolved aerosol particles which  
178 can be analyzed by various methods. Each PILS system sampled from ~~a~~their own Submicron  
179 Aerosol Inlet (SMAI) [Craig *et al.*, 2013a, 2013b, 2014; Moharreri *et al.*, 2014] mounted to the  
180 belly of the NSF/NCAR C-130. The size-cut for each PILS was provided by a nonrotating  
181 MOUDI impactor stage with a 50% transmission efficiency of 1  $\mu\text{m}$  aerodynamic diameter (i.e.,  
182  $\text{PM}_{10}$ ) at 1 atmosphere ambient pressure [Marple *et al.*, 1991]. The flowrate of 15 LPM was  
183 sampled by

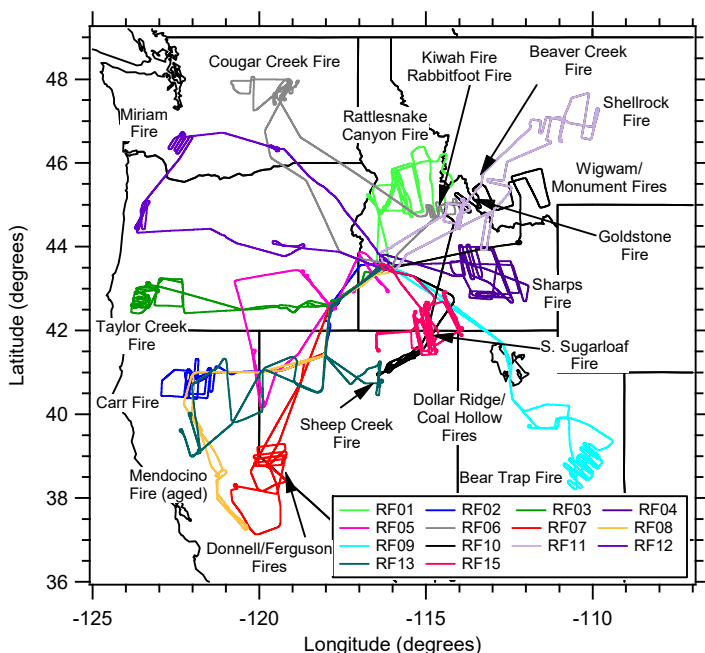


Figure 1. Map showing the flight paths and locations of the wildfires sampled during WE-CAN used in this analysis.

184  
185  
186

each PILS through the inlet and MOUDI stage. An activated carbon parallel plate denuder [Eatough *et al.*, 1993] was situated upstream of both PILS to remove organic gases. In addition, for PILS2 two honeycomb denuders coated with sodium carbonate and phosphorous acid were used to remove inorganic acidic and basic gases in order to limit possible positive artifacts from dissolving in the PILS collection liquid. PILS 1 was connected to a LWCC (liquid waveguide capillary cell) and TOC (Total Organic Carbon) Analyzer for near real-time measurement of water-soluble BrC (Brown Carbon) absorption and WSOC (water-soluble organic carbon), respectively. PILS2 was coupled to a Bretchel fraction collector system [Sorooshian *et al.*, 2006] to provide liquid samples for additional off-line analysis.

196  
197  
198  
199

For PILS 1, a valve upstream of the PILS was manually closed periodically for 10 min forcing the airflow through a Teflon filter allowing for a measurement of the background in near real-time. The liquid sample obtained from PILS1 was then pushed through a 0.2  $\mu\text{m}$  PTFE liquid filter at a flowrate of 1.2 mL/min by a set of syringe pumps with 1 mL syringes to ensure any insoluble particles were removed before passing through the LWCC and TOC Analyzer.

201  
202  
203

A LWCC with a 2.5 m path-length (World Precision Instruments, Sarasota, FL) was employed. An absorption spectrometer (FLAME-T-UV-VIS, Ocean Optics, Largo, FL) and dual deuterium and tungsten halogen light source (DH-mini, Ocean Optics, Largo, FL) were coupled

204 to the LWCC via fiber optic cables. The Oceanview Spectroscopy Software was used to record  
205 absorption spectra over a range from 200 to 800 nm. In this paper we present the absorption  
206 determined at 365 and 405 nm. This wavelength dependent absorption was calculated following  
207 the method outlined in *Hecobian et al.* [2010]. A 16 s integrated measurement of water-soluble  
208 absorption with a limit of detection (LOD) of  $0.1 \text{ Mm}^{-1}$  was obtained.

209 A Sievers Model M9 Portable TOC Analyzer (Suez Waters Analytical Instruments,  
210 Boulder, CO) was used for the WSOC measurement. This analyzer converts organic carbon in  
211 the liquid sample to carbon dioxide using chemical oxidation with ammonium persulfate and  
212 ultraviolet light. The carbon dioxide formed is then measured by conductivity. The amount of  
213 OC present in the sample is proportional to the increase in conductivity observed. The analyzer  
214 was run in turbo mode providing a 4 s integrated measurement of WSOC with a LOD of  $0.1 \mu\text{g}$   
215  $\text{C}/\text{m}^3$ .

216 For PILS2, a valve upstream of the PILS was manually closed periodically for 10 min  
217 forcing the airflow through a hepa filter allowing for measurement of the background in near  
218 real-time. The liquid sample obtained from PILS2 was pushed into the fraction collector vials at  
219 a flowrate of  $0.65 \text{ mL}/\text{min}$  by a peristaltic pump for collection of  $\sim 1.2 \text{ mL}$  of liquid sample per  
220 vial. Each fraction collector carousel holds 72  $1.5 \text{ mL}$  polypropylene vials (Microsolv  
221 Technology Corporation, Leland, NC). Vials were fitted with pre-slit caps and used as supplied.  
222 The fraction collector program was set to allow continuous collection of 2 min integrated  
223 samples and was manually started after take-off. Carousels were pre-loaded before flight and  
224 then manually switched out as they were filled. The vials were unloaded from the carousels at  
225 the end of each flight, recapped with solid caps (Microsolv Technology Corporation), packed in  
226 coolers with ice packs, and shipped back to Colorado State University to be stored in a  $2 \text{ }^\circ\text{C}$  cold  
227 room until analysis began following completion of the study.  
228

### 229 2.3. Off-line Analysis

230 Each fraction collector vial was brought to room temperature and then analyzed for  
231 levoglucosan as well as ~~as a suite of anions/organic acids and~~ cations. For each analysis,  $300 \mu\text{L}$   
232 aliquots were transferred to polypropylene vials. Only levoglucosan, water-soluble potassium,  
233 and ammonium are discussed here and their analytical methods are explained below.

234 The levoglucosan analysis was performed on a Dionex DX-500 series ion chromatograph  
235 with pulsed amperometric detection via an ED-50/ED-50A electrochemical cell. This cell  
236 includes two electrodes: a "standard" gold working electrode and pH-Ag/AgCl (silver/silver  
237 chloride) reference electrode. A sodium hydroxide gradient and a Dionex CarboPac PA-1  
238 column ( $4 \times 250 \text{ mm}$ ) were employed for the separation. The complete run time was 59 min  
239 with an injection volume of  $100 \mu\text{L}$ . More details on the method can be found in *Sullivan et al.*  
240 [2011a,b, 2014, 2019]. Only levoglucosan could be detected in the WE-CAN samples (other less  
241 abundant anhydrosugars were too low to detect in the PILS samples) and did not require  
242 background correction. The LOD for levoglucosan based on a sample collection time of 2 min  
243 and air flowrate of 15 LPM was determined to be less than approximately  $0.10 \text{ ng}/\text{m}^3$ .

244 A Dionex ICS-3000 ion chromatograph ~~equipped with a conductivity detector~~ was used  
245 to measure water-soluble potassium and ammonium. An eluent generator provided a  
246 concentration of  $20 \text{ mM}$  methanesulfonic acid at a flowrate of  $0.5 \text{ mL}/\text{min}$  to perform the  
247 separation on a Dionex IonPac CS12A analytical column ( $3 \times 150 \text{ mm}$ ). The complete run time  
248 was 17 min with an injection volume of  $190 \mu\text{L}$ . A blank correction was necessary for both of  
249 these species unlike levoglucosan. Therefore, their concentrations were corrected by using the

250 average of all background samples collected during a specific flight. For water-soluble  
251 potassium and ammonium, the LOD was 1 ng/m<sup>3</sup>.

#### 253 **2.4. Photoacoustic Aerosol Absorption Spectrometer**

254 A custom-built PAS was used to measure total aerosol absorption at 405 and 660 nm  
255 [Foster *et al.*, 2019] every 1 s during WE-CAN. The PAS measures aerosol light absorption at  
256 near-ambient conditions by heating particles using a controlled light source and detecting the  
257 resulting soundwave. It can be subject to interference by gaseous absorbers and is sensitive to  
258 variations in relative humidity, temperature, and pressure [Arnott *et al.*, 1999; Langridge *et al.*,  
259 2013]. The PAS sampled from a Solid Diffuser Inlet (SDI) mounted on the front right side of the  
260 NSF/NCAR C-130. Aerosol passed through a cyclone impactor before entering the PAS to  
261 remove particles with aerodynamic diameters > 1 µm. The flowrate for the PAS was 4 LPM.  
262 Upstream of the PAS was a denuder to remove NO<sub>x</sub> (nitrogen oxides) from the sample air as  
263 well as a Perma Pure dryer to dry the aerosol to below 30% relative humidity. A filter was  
264 periodically switched in-line before the PAS to remove particles and allow for a near real-time  
265 measurement of the baseline stability. Additionally, the PAS switched between sampling with  
266 and without a thermal denuder system in-line. Only the data from sampling without the thermal  
267 denuder is presented here. The PAS BrC absorption at 405 nm (PAS total Abs 405 BrC) was  
268 calculated using equation 9 from Pokhrel *et al.* [2017]. This approach assumes the absorption  
269 determined by the PAS at 660 nm was equivalent to BC absorption and the BC aerosol AAE was  
270 1, and the absorption enhancement from lensing was constant at all wavelengths. Previous work  
271 using this approach in smoke from controlled laboratory burns found lensing could contribute a  
272 maximum of 30% of total absorption, but typical contributes much less.-

#### 274 **2.5. Ultra-High-Sensitivity Aerosol Spectrometer**

275 One second particle number concentrations were measured using a rack-mounted  
276 UHSAS (Ultra-High-Sensitivity Aerosol Spectrometer). The rack-mounted UHSAS switched  
277 between sampling from the SDI inlet and a CVI (counter-flow virtual impactor) when sampling  
278 out of and in-cloud, respectively. We only present data for sampling out of clouds. The rack-  
279 mounted UHSAS was operated so that the flow could be manually lowered by the in-flight  
280 operator when the NSF/NCAR C-130 flew through smoke plumes to allow the UHSAS to stay  
281 within its optimum concentration measurement range. The UHSAS measures particles in the  
282 0.06-1 µm range. The particle size bins for the UHSAS were calibrated using ammonium sulfate  
283 rather than traditional PSL (polystyrene latex) spheres. Particle mass concentrations for PM<sub>1</sub>  
284 were calculated by applying these summing all size bins and then multiplying by 1.4 g/cm<sup>3</sup> to  
285 account for particle density.

#### 287 **2.6. Other Measurements**

288 In the following analysis, we focus on characterizing the BrC absorption in smoke from  
289 wildfires in the western U.S. sampled during WE-CAN. Other airborne measurements used in  
290 this analysis include meteorological data and coordinates provided by the Research Aviation  
291 Facility (RAF) as part of the C-130 instrumentation package  
292 (<https://data.eol.ucar.edu/project/WE-CAN>) and one Hz carbon monoxide (CO) determined by a  
293 vacuum UV (ultraviolet) resonance fluorescence method [Gerbig *et al.*, 1999]. All data  
294 presented in our analysis are reported at 1 atm and 273 K. Data from all species have been  
295 averaged to match the 2 min collection time of the PILS-fraction collector system.

296  
297  
298  
299  
300  
301  
302

## 2.7. Mie Calculation

Mie calculations were performed by putting the complex refractive index ( $m = n + ik$ ) into Mie code to obtain the absorption efficiency ( $Q$ ) and then further calculate the absorption coefficient using Eq. 1 [Liu *et al.*, 2013]. The real part of the refractive index ( $n$ ) was set to be 1.55 and the imaginary part was calculated using Eq. 2 [Liu *et al.*, 2013].

$$\beta(\lambda, D_p) = \frac{3}{2} \cdot \frac{Q \cdot WSOC}{D_p \cdot \rho} \quad (Eq. 1)$$

304

$$k = \frac{\rho \lambda \cdot H_2O\_ \beta(\lambda)}{4\pi \cdot WSOC} \quad (Eq. 2)$$

306

In Eq. 1 and 2,  $\lambda$  is the wavelength,  $D_p$  is the diameter of the particle,  $\beta$  is the absorption coefficient (referred to as the Mie calculated water-soluble absorption hereinafter),  $Q$  is the absorption efficiency,  $WSOC$  is the water-soluble organic carbon mass concentration measured by the PILS, and  $H_2O\_ \beta(\lambda)$  is the water-soluble light absorption coefficient measured by the PILS. The particle density ( $\rho$ ) was assumed to be 1.4 g/cm<sup>3</sup>. The plume averaged particle size distribution (measured by the UHSAS) was used in the calculation. The Mie calculated water-soluble absorption was determined for each size bin in order to obtain the most accurate results. Mie calculated total absorption was further calculated by multiplying the Mie calculated water-soluble absorption by (UHSAS mass)/(WSOC\*1.6), where the factor of 1.6 was to convert WSOC to WSOM (water-soluble organic matter) [Duarte *et al.*, 2019; Yttri *et al.*, 2007].

317

## 3. Results and Discussion

318

### 3.1. Overview

319

Most previous studies employing a LWCC to determine water-soluble absorption, examine the absorption at 365 nm (e.g., [Hecobian *et al.*, 2010; Zhang *et al.*, 2011, 2013]. But here in order to explore the relationship between the water-soluble and total absorption determined by the PILS and PAS, respectively, we focus on the absorption at 405 nm determined by the LWCC. Using as examples Flight RF02, which sampled the Carr Fire smoke plume, and Flight RF11, which sampled the Goldstone, Rabbit Foot, Beaver Creek, and Shellrock Fire smoke plumes, Figures 2a and b show the relationship of the PILS water-soluble Abs 405 vs. Abs 365. Absorption values at these two wavelengths are correlated ( $R^2$  values from 0.70 to 1.00 based on all individual WE-CAN Flights), but the absorption measured at 405 nm was about half of that observed at 365 nm (slope average 0.45 and range from 0.39 to 0.52 across all individual WE-CAN flights). We selected these two flights to cover the range in the relationships observed during WE-CAN. The lower correlation for Flight RF11 is likely due to the narrower plumes being sampled compared to the broader plumes observed in Flight RF02. This difference related to narrow vs. broad plumes was observed throughout the various wildfires sampled during WE-CAN.

335

Figure 3 shows example time series for WSOC, PILS water-soluble Abs 405, and PAS total Abs 405 BrC from the same two flights as above. It was observed that all three parameters tracked each other in and out of the smoke plumes. During WE-CAN, the average value  $\pm$  standard deviation for WSOC, PILS water-soluble Abs 405, and PAS total Abs 405 BrC were

336  
337  
338



339  $13.35 \pm 16.80 \mu\text{g C/m}^3$ ,  $6.06 \pm 6.88 \text{ Mm}^{-1}$ , and  $22.02 \pm 49.16 \text{ Mm}^{-1}$ , respectively. The water-  
340 soluble absorption determined by the PILS was lower than the total absorption determined by the  
341 PAS. This pattern was consistently observed for all the wildfires sampled throughout WE-CAN.  
342  
343  
344

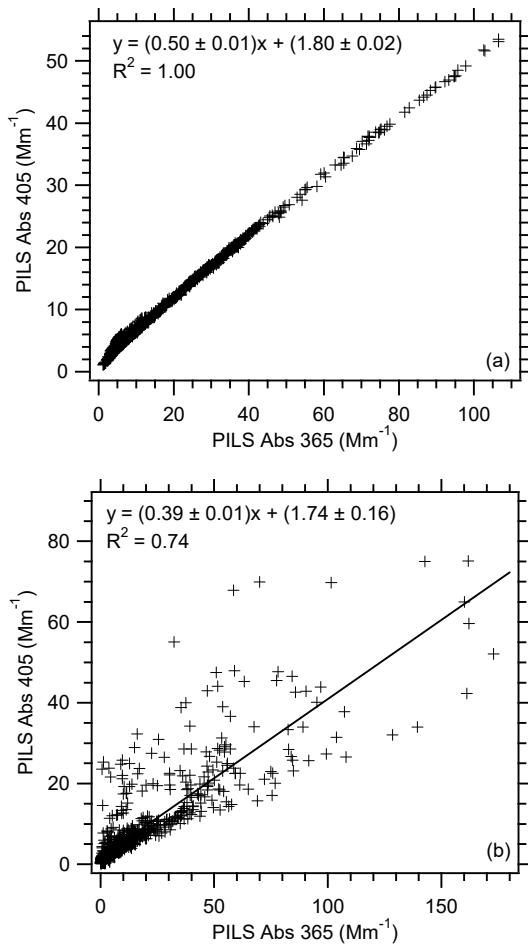


Figure 2. Correlation of PILS water-soluble Abs 405 vs. PILS water-soluble Abs 365 for WE-CAN (a) Flight RF02 and (b) Flight RF11. Uncertainties with the least square regressions are one standard deviation.

345  
346

347  
348  
349  
350  
351  
352

### 3.2. Relationship between Total and Water-Soluble BrC Absorption

To further explore the relationship between total and water-soluble BrC absorption, we examine the relationship between PAS total Abs 405 BrC and UHSAS mass for Flights RF02 and RF11. There is a strong correlation between PAS total Abs 405 BrC and UHSAS mass (Figure 4). Therefore, the PILS water-soluble Abs 405 can be corrected for the non-water-

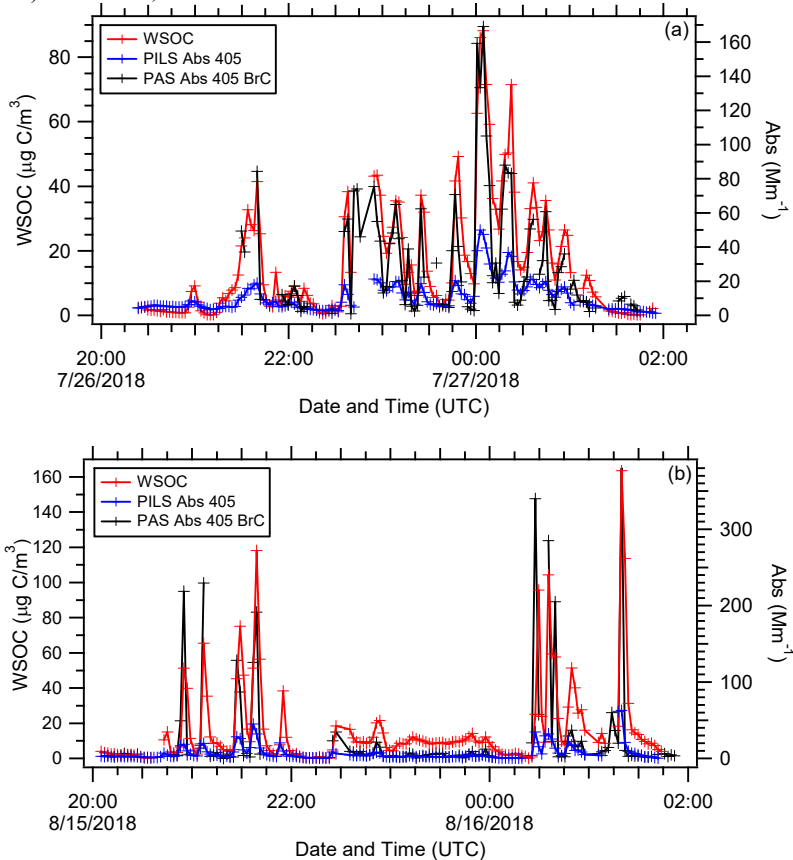


Figure 3. Time series of WSOC, PILS water-soluble Abs 405, and PAS total Abs 405 BrC for WE-CAN (a) Flight RF02 and (b) Flight RF11.

353  
354  
355  
356  
357  
358

soluble fraction of the aerosol using the UHSAS mass. This was achieved by multiplying the PILS water-soluble Abs 405 by  $1/((\text{WSOC} \cdot 1.6)/(\text{UHSAS mass}))$  or  $(\text{UHSAS mass})/(\text{WSOC} \cdot 1.6)$ . This approach assumes the water-soluble and characteristics of the non-

359 water-soluble components of OC are identical to that of the water-soluble components of OC  
 360 are the same.

361 Correcting the PILS water-soluble Abs 405 by the UHSAS mass showed good closure  
 362 with the PAS total Abs 405 BrC, but with a factor of ~1.5 to 2 difference between the PILS  
 363 water-soluble Abs 405 corrected and PAS total Abs 405 BrC (Figures 4c and d). This is also  
 364 similar to results obtained from the sampling of wildfire smoke during the FIREX (Fire Influence  
 365 on Regional and Global Environments Experiment) Campaign, where there was a ratio of 3.2  
 366 between PAS Abs 405 BrC and water-soluble Abs 405 determined from off-line LWCC analysis

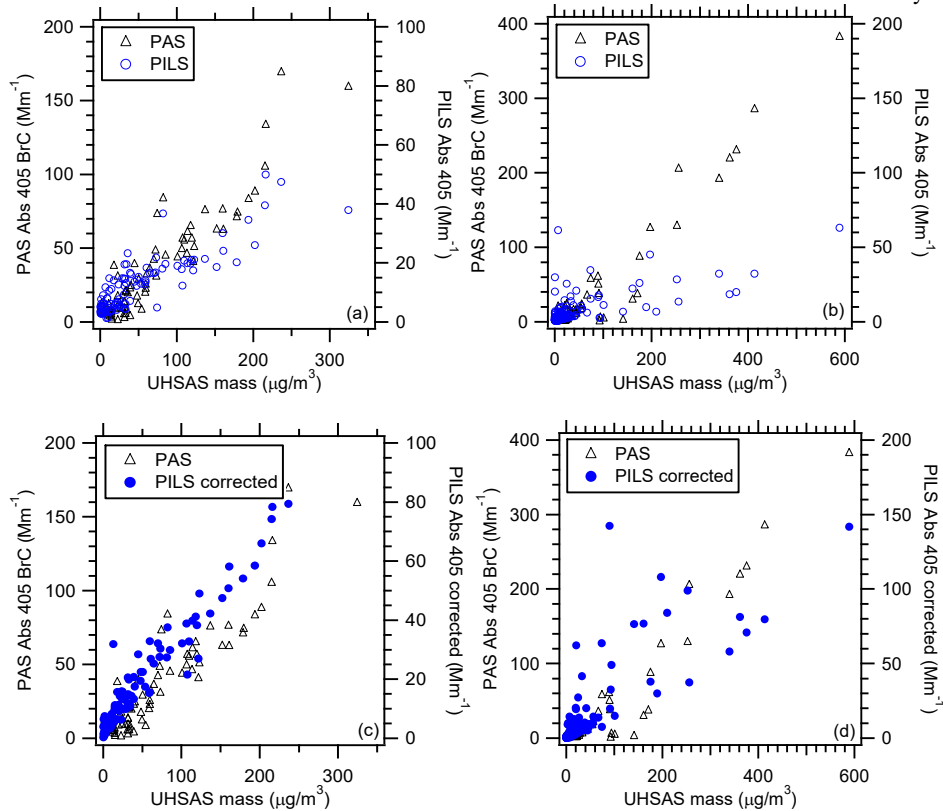


Figure 4. Correlation of PAS total Abs 405 BrC and PILS water-soluble Abs 405 vs. UHSAS mass for WE-CAN (a) Flight RF02 and (b) Flight RF11. Correlation of PAS total Abs 405 BrC and PILS water-soluble Abs 405 corrected for the non-water-soluble fraction of the aerosol using the UHSAS mass for WE-CAN (c) Flight RF02 and (d) Flight RF11. In plot (a), the equations for the fit and  $R^2$  value for PAS are  $y = (0.50 \pm 0.02)x - (0.03 \pm 2.29)$ ,  $R^2 = 0.87$  and for PILS are  $y = (0.14 \pm 0.01)x + (5.58 \pm 0.65)$ ,  $R^2 = 0.75$ , respectively. In plot (b), the equations for the fit and  $R^2$  value for PAS are  $y = (0.62 \pm 0.03)x - (6.09 \pm 3.62)$ ,  $R^2 = 0.76$  and for PILS are  $y = (0.08 \pm 0.01)x + (3.58 \pm 0.66)$ ,  $R^2 = 0.43$ , respectively. In plot (c), the equation for the fit and  $R^2$  value for PILS are  $y = (0.32 \pm$

$0.01)x + (3.60 \pm 0.68)$ ,  $R^2 = 0.94$ , respectively. In plot (d), the equation for the fit and  $R^2$  value for PILS are  $y = (0.24 \pm 0.01)x + (2.93 \pm 1.35)$ ,  $R^2 = 0.65$ , respectively. Uncertainties with the least square regressions are one standard deviation.

367  
368  
369

370 of filter samples [Zeng *et al.*, 2020]. This factor difference in both the WE-CAN and FIREX  
371 data is likely due to the differences in particle vs. bulk solution absorption measured by the PAS  
372 vs. LWCC (using PILS or filter samples), respectively, and can be explained by Mie Theory.

373 We used Mie Theory to calculate the water-soluble and total particle Abs 405 (see section  
374 2.7 for details on the equations and parameters used) through each plume transect for RF02 and  
375 RF11. As shown in Figures 5a and b, we found a slope of 1.7 to 1.8 for Mie calculated water-  
376 soluble Abs 405 to PILS Abs 405 and 3 to 4 for Mie calculated total Abs 405 to PILS Abs 405.  
377 This is similar to results presented in Liu *et al.* [2013] and based on off-line LWCC analysis of  
378 filter samples collected at 3 sites in Georgia. In that work, a ratio of 2 for Mie calculated water-  
379 soluble Abs 365 to measured water-soluble Abs 365 and a ratio of 3.6 for Mie calculated total  
380 Abs 365 to measured water-soluble Abs 365 were observed. In Zeng *et al.* [2022], Mie Theory  
381 was used to calculate the factor to convert solution to particle light absorption (i.e., ratio of Mie  
382 calculated to measured water-soluble absorption) as a function of wavelength for the FIREX  
383 data. At 405 nm a factor of ~1.7 was determined, similar to what was determined from the WE-  
384 CAN data.

385 As a further check on the calculations performed here, the PAS Abs 405 BrC was  
386 compared to the Mie calculated total Abs 405. Slopes ranged from 1.04 to 1.08 (Figures 5c and  
387 d). This suggested our approach for correcting the PILS water-soluble Abs 405 for the non-  
388 water-soluble fraction as well as to calculate the BrC absorption from the PAS Abs 405 data  
389 were valid.

390 Overall, during WE-CAN ~45% (ranging from 31% to 65%) of the BrC absorption at  
391 Abs 405 was due to water-soluble species. This is similar to what was observed from off-line  
392 LWCC analysis of water and methanol extracts from filter samples collected during sampling of  
393 biomass burning plumes as part of the DC3 (Deep Convective Clouds and Chemistry),  
394 SEAC4RS (Studies of Emissions, Atmospheric Composition, Clouds and Climate Coupling by  
395 Regional Surveys), and FIREX aircraft campaigns [Forrister *et al.*, 2015; Liu *et al.*, 2015; Zeng  
396 *et al.*, 2022].

397

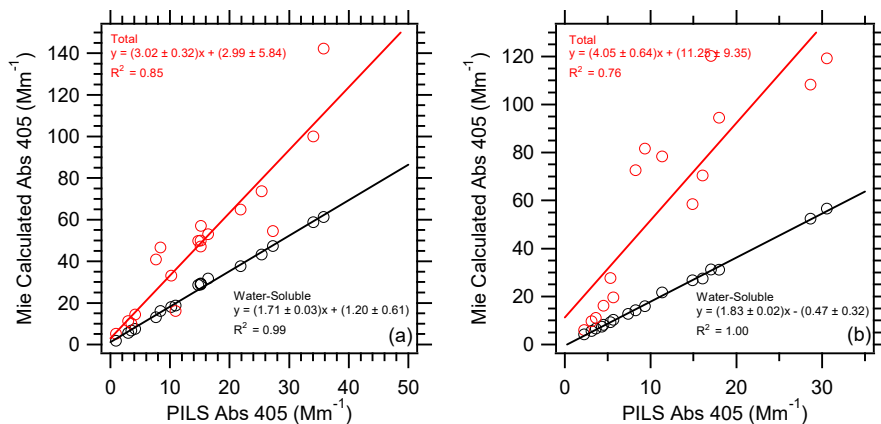
### 398 **3.3. BrC Absorption, CO, WSOC, and Levoglucosan**

399 Using data from all WE-CAN flights, Figure 6 shows that the PAS total Abs 405 BrC and  
400 PILS water-soluble Abs 405 are correlated with CO ( $R^2$  value for PAS = 0.76 and PILS = 0.55).  
401 This further illustrates the importance of biomass burning as a source of BrC absorption (e.g.,  
402 [Andreae and Gelencsér, 2006; Chakrabarty *et al.*, 2010; Duarte *et al.*, 2005; Hecobian *et al.*,  
403 2010; Hoffer *et al.*, 2006; Lack *et al.*, 2012; Lukács *et al.*, 2007]), especially since more than  
404 75% of the WE-CAN data occurred in smoke.

405 Figure 7 shows that there is a correlation between BrC absorption and WSOC ( $R^2$  value  
406 for PAS = 0.42 and PILS = 0.60). This is not surprising given that the two main sources of  
407 WSOC are typically biomass burning and secondary organic aerosol (SOA) [Sullivan *et al.*,  
408 2006]. A number of previous studies where the source of WSOC and Abs 365 was one or both  
409 of these have observed a similar correlation (e.g., [Hecobian *et al.*, 2010; Liu *et al.*, 2015; Zhang

410 *et al.*, 2013]). Additionally, analysis of cloud water samples impacted by biomass burning has  
 411 shown that nitrophenols and nitrocatechol are major contributors to the light absorption between  
 412 300 and 400 nm [Desyaterik *et al.*, 2013].

413 BrC absorption has a similar relationship with CO and WSOC as the biomass burning  
 414 marker levoglucosan [Simoneit *et al.*, 1999], but there are additional features (Figures 8a and b).  
 415 There is some variability in the ratio of levoglucosan to the PAS total Abs 405 BrC and PILS  
 416 water-soluble Abs 405 between wildfires, and this leads to two branches (Branch 1 and Branch  
 417 2). This was also observed for levoglucosan vs. WSOC (not shown). While there is no overall  
 418 correlation of levoglucosan vs. BrC absorption across all flights, there are correlations between  
 419 these two species on an individual flight basis (e.g.,  $R^2$  value for Flight RF02 = 0.76 and Flight  
 420 RF11 = 0.60, not shown). When data from all flights are colored by the water-soluble potassium  
 421 concentration (Figures 8c and d), we observe that Branch 1, which had the highest levoglucosan  
 422 concentrations, also has the highest water-soluble potassium concentrations ( $> 0.5 \mu\text{g}/\text{m}^3$ ).  
 423 Levoglucosan and BrC absorption are much more highly correlated in Branch 1, than in Branch  
 424 2 for both the PILS ( $R^2$  values Branch 1 = 0.76 and Branch 2 = 0.35) and PAS ( $R^2$  values Branch  
 425 1 = 0.60 and Branch 2 = 0.22) BrC absorption. To further examine this, the times series of PILS  
 426



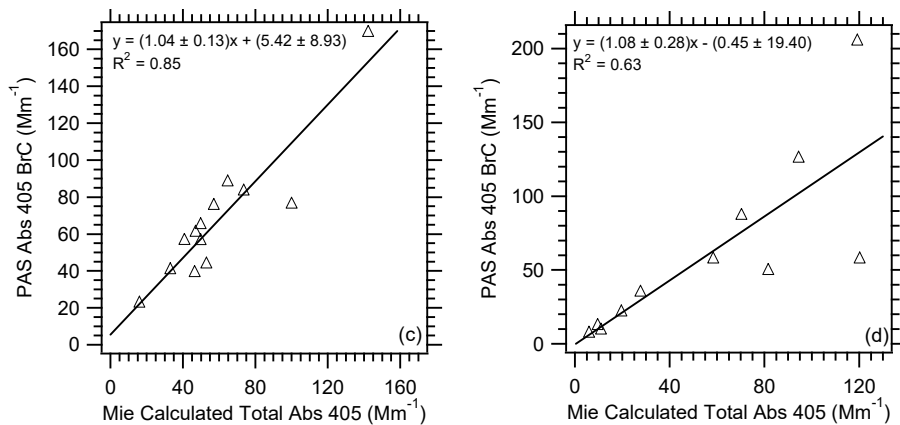


Figure 5. Correlation of Mie calculated water-soluble and total Abs 405 vs. PILS water-soluble Abs 405 for WE-CAN (a) Flight RF02 and (b) Flight RF11. Correlation of PAS total Abs 405 BrC and Mie calculated total Abs 405 for WE-CAN (c) Flight RF02 and (d) Flight RF11. Uncertainties with the least square regressions are one standard deviation.

427  
 428  
 429  
 430 water-soluble Abs 405, levoglucosan, potassium, and ammonium for Flights RF02 and RF11 are  
 431 shown in Figure 9. Smoke impacted samples in Flight RF02 had higher concentrations of  
 432 levoglucosan and water-soluble potassium and contributed to Branch 1. The data from Flight  
 433 RF11 contributed to Branch 2. In addition, elevated water-soluble potassium was observed in  
 434 many of the plume intercepts during Flight RF02. But more elevated ammonium was observed  
 435 for Flight RF11, which became even more prominent in smoke intercepts after 00:00 UTC, while  
 436 water-soluble potassium was relatively less abundant. While ammonium was clearly more  
 437 prominent, there was no correlation observed between ammonium and PAS total Abs 405 BrC or  
 438 PILS water-soluble Abs 405 for the data contributing to Branch 2 (not shown). Water-soluble  
 439 potassium is a known

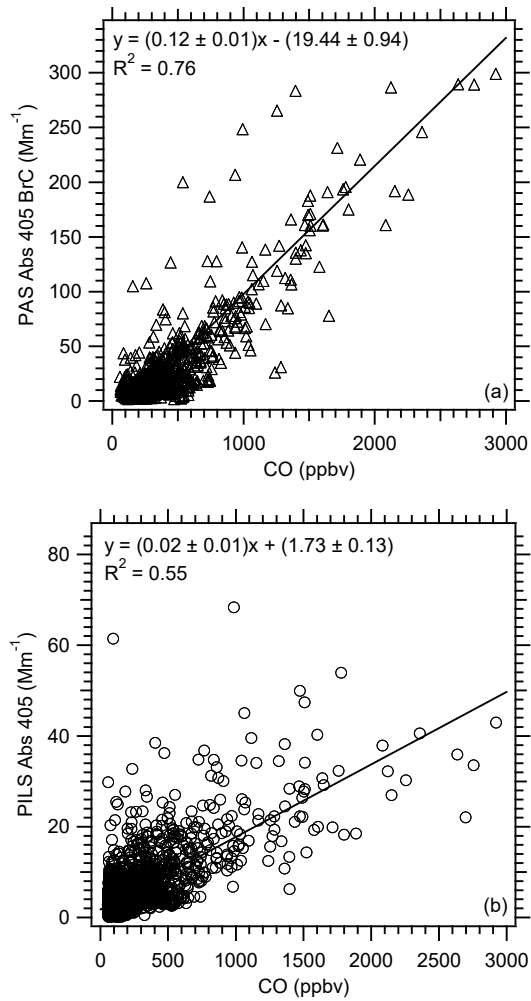


Figure 6. Correlation of (a) PAS total Abs 405 BrC and (b) PILS water-soluble Abs 405 vs. CO for all WE-CAN flights used in this analysis. Uncertainties with the least square regressions are one standard deviation.

440  
441  
442  
443  
444  
445

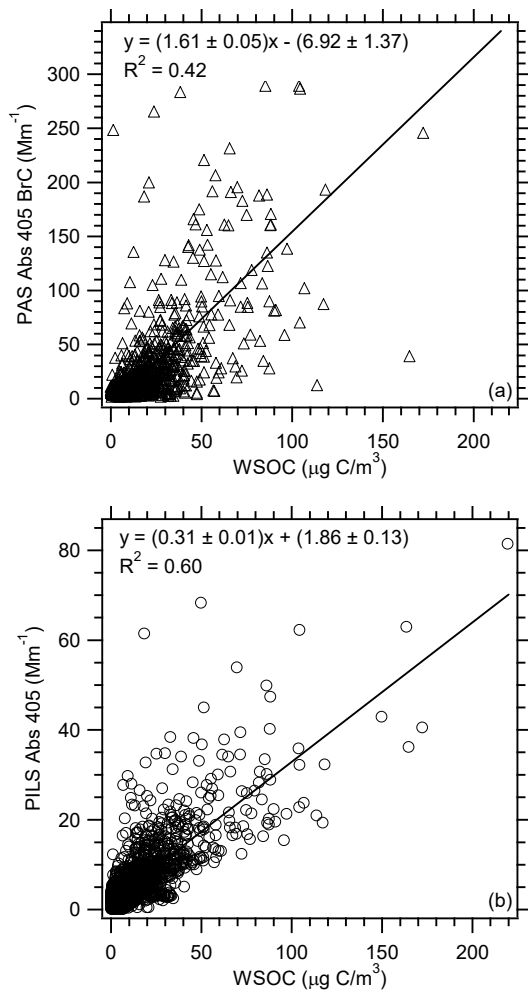
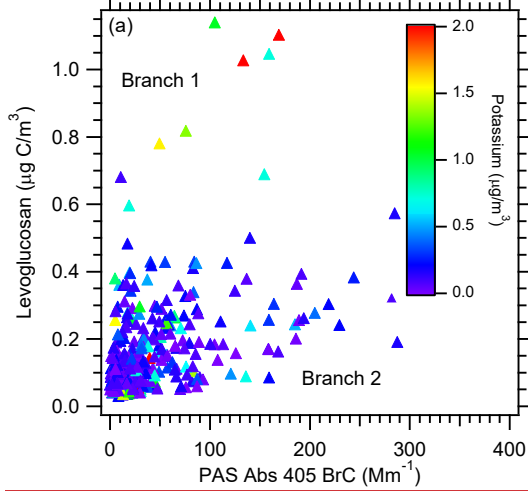
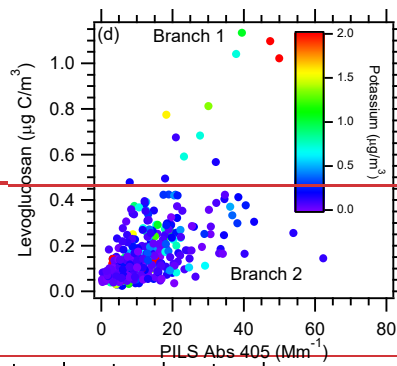
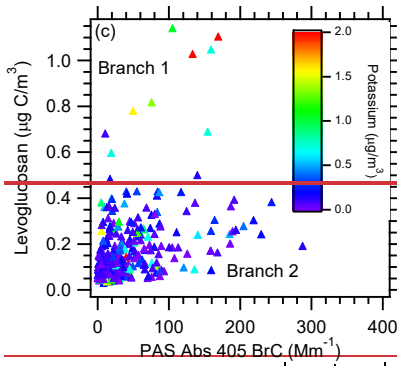
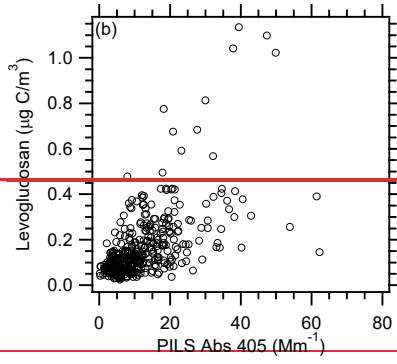
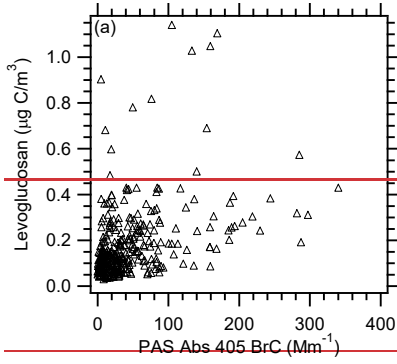
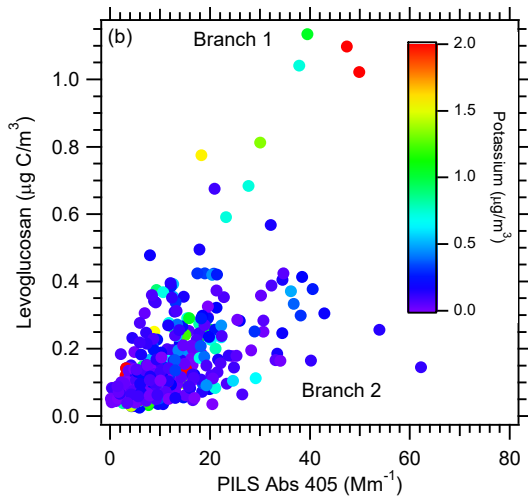


Figure 7. Correlation of (a) PAS total Abs 405 BrC and (b) PILS water-soluble Abs 405 vs. WSOC for all WE-CAN flights used in this analysis. Uncertainties with the least square regressions are one standard deviation.

446  
 447  
 448  
 449  
 450  
 451







Formatted: Centered

Figure 8. Correlations of levoglucosan on a carbon mass basis vs. (a) PAS total Abs 405 BrC and (b) PILS water-soluble Abs 405 for all WE-CAN flights used in this analysis. ~~Plots (e) and (d) are the same as plots (a) and (b), but~~ with the data colored by the PILS water-soluble potassium concentrations. Branch 1 represents data with water-soluble potassium concentrations  $> 0.5 \mu\text{g}/\text{m}^3$  and Branch 2  $< 0.5 \mu\text{g}/\text{m}^3$ . In plot (ae), the equation for the fit and  $R^2$  value for Branch 1 are  $y = (0.006 \pm 0.001)x + (0.027 \pm 0.049)$ ,  $R^2 = 0.60$  and for Branch 2  $y = (0.001 \pm 0.001)x + (0.118 \pm 0.006)$ ,  $R^2 = 0.22$ , respectively. In plot (be), the equation for the fit and  $R^2$  value for Branch 1 are  $y = (0.024 \pm 0.002)x - (0.081 \pm 0.038)$ ,  $R^2 = 0.76$  and for Branch 2  $y = (0.006 \pm 0.001)x + (0.073 \pm 0.007)$ ,  $R^2 = 0.35$ , respectively. Uncertainties with the least square regressions are one standard deviation.

452  
 453  
 454  
 455 inorganic marker for biomass burning, although it is not as specific of a marker as levoglucosan  
 456 as there are additional possible sources for water-soluble potassium [Schauer et al., 2001] and  
 457 water-soluble potassium is predominately emitted during only the flaming phase of a fire [Lee et  
 458 al., 2010]. It is possible this difference in timing of emissions is what leads to the different  
 459 relationship of Abs 405 with levoglucosan than was observed for CO and WSOC. It has been  
 460 observed in previous work looking at the size-resolved aerosol composition and single particle  
 461 measurements from wildfire plumes that water-soluble potassium and levoglucosan appear in  
 462 different sized particles than BrC and that there is non-uniform mixing of them [Di Lorenzo et  
 463 al., 2018; Lee et al., 2016], which could also be a factor. These results from WE-CAN are  
 464 further suggesting there may be a relationship between levoglucosan and water-soluble  
 465 potassium in wildfire emissions that has not been observed in other types of burning, such as  
 466 prescribed burning, residential burning, and controlled laboratory burns [Sullivan et al., 2014,  
 467 2019].

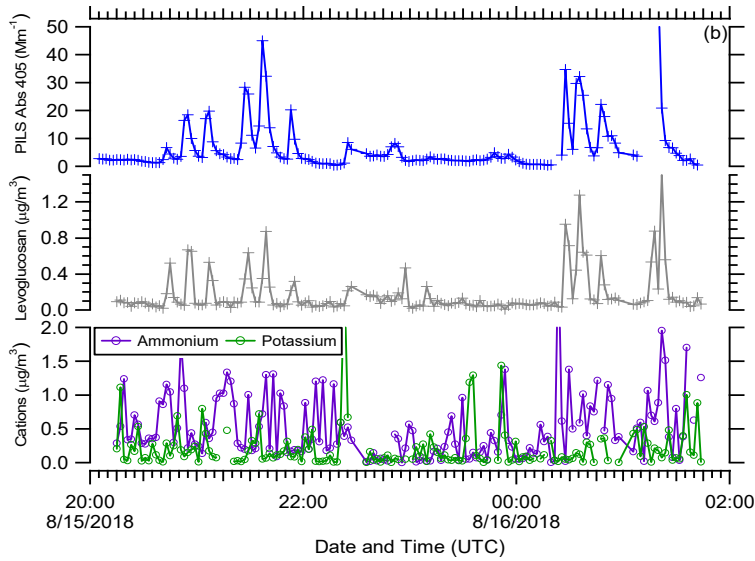
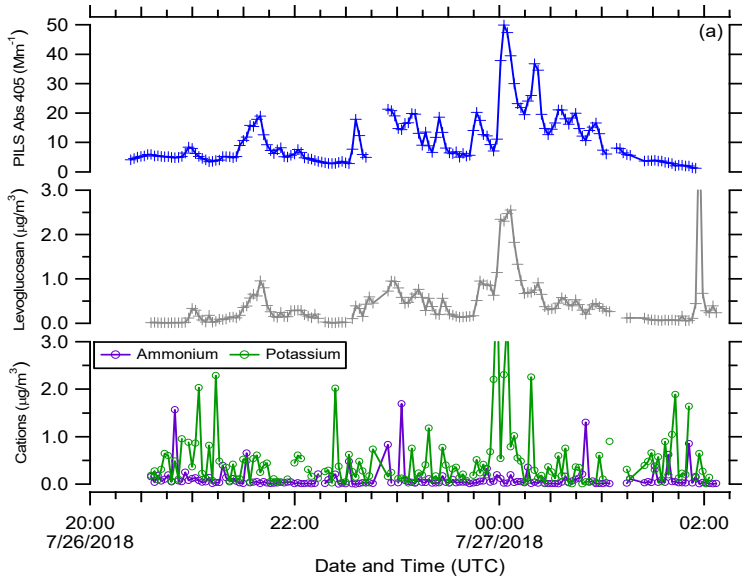


Figure 9. Time series from top to bottom of PILS water-soluble Abs 405, PILS levoglucosan, and PILS ammonium and water-soluble potassium for WE-CAN (a) Flight RF02 and (b) Flight RF11.

#### 3.4. Evolution of BrC Absorption with Plume Age and Fire Dynamics

The time since emission (i.e., the smoke age) was estimated for all possible wildfire plumes as the distance the plume was sampled from the source divided by the average wind speed at that particular sampling altitude. Only PILS-fraction collector samples that directly overlapped with a CO plume penetration are considered. To account for dilution, we normalized the BrC absorption to 3 different species. We examine the ratio of BrC absorption to WSOC,  $\Delta\text{CO}$  (assuming a CO background of 100 ppbv), and levoglucosan.

Figure 10a presents the ratio of PAS total Abs 405 BrC to WSOC and PILS water-soluble Abs 405 to WSOC, Figure 10b presents the ratio of PAS total Abs 405 BrC to  $\Delta\text{CO}$  and PILS water-soluble Abs 405 to  $\Delta\text{CO}$ , and Figure 10c presents the ratio of PAS total Abs 405 BrC to levoglucosan and PILS water-soluble Abs 405 to levoglucosan as a function of time since emission. To better discern any trends, Figures S1-S3 show these 3 ratios for each smoke plume individually by flight basis. If WSOC was lost with age due to evaporation of more volatile components or SOA formation were occurring with time since emission, CO would be expected to be more stable. It appears, however, that a similar pattern, perhaps with a bit more scatter for Abs 405 to WSOC, is observed for all of these ratios. Within a particular wildfire, there is no clear evidence that the PILS water-soluble BrC absorption is affected by smoke age up to 9 h. For the PAS total BrC absorption, especially for the ratio to  $\Delta\text{CO}$ , there appears to be a possible decrease in the ratio in the first 2 h (see Figures S1i and S2i for Flight RF15 which best covered this period), suggesting a need to further explore changes in total BrC absorption near the source region.

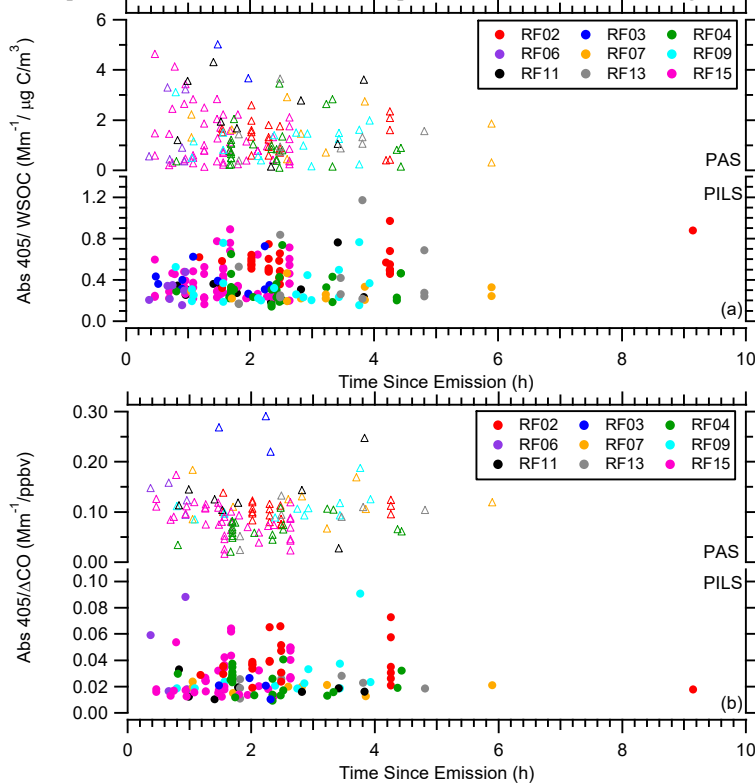
A number of laboratory studies suggest the initial stages of photochemical aging increases light absorption (i.e., photoenhancement). This is then followed by a decrease in light absorption (i.e., photobleaching) [Hems and Abbatt, 2018; Saleh et al., 2013; Sumlin et al., 2017; Zhao et al., 2015; Zhong and Jang, 2014]. However, it is challenging to directly compare this laboratory data to the ambient data collected during WE-CAN. But analysis of laboratory and ambient biomass burning samples by Wong et al. [2019], found low molecular weight (< 400 Da) BrC undergoes rapid photobleaching on timescales of a few h, but high molecular weight (> 400 Da) BrC was stable for up to a few days [Di Lorenzo et al., 2017; Wong et al., 2019]. This suggests that the BrC sampled during WE-CAN could be composed mainly of high molecular weight species.

In addition, to investigate these ratios as a function of time since emission, the WE-CAN data had to be integrated across a smoke plume in order to incorporate the PILS-fraction collector measurements. Of course, a smoke plume itself was dynamic with concentrations being highest in the middle of the plume and more dilute on the edges. It is possible the averaging could contribute to the observed pattern of BrC absorption not changing with age. Forrister et al. [2015], who used plume transect averages of SEAC4RS data, reported a decrease in the total Abs 365/ $\Delta\text{CO}$  from  $\sim 0.13$  to  $0.07 \text{ Mm}^{-1}/\text{ppbv}$  in 5 h for smoke from the Rim Fire. Observations of smoke during FIREX, by contrast, indicated no clear trend with plume age [Washenfelder et al., 2022; Zeng et al., 2022] in a dataset where the majority of plume ages were less than 10 h. These varying results also suggest that other factors that contribute to changes in BrC absorption over time may still need to be explored.

As these three studies all examined Abs 365, the same series of plots shown in Figure 10 are repeated for PILS water-soluble Abs 365 and shown in Figure S4. A similar pattern was observed at both wavelengths for the WE-CAN data. This suggests our results were not wavelength specific and further corroborate the results observed during FIREX.

515 An analysis of WE-CAN data by Palm et al. [2020] looking at the evolution of organic  
 516 aerosol and BrC suggested that although changes in organic aerosol were likely occurring, there  
 517 was a balance between dilution-driven evaporation and subsequent formation resulting in little  
 518 change over time. It is hard to compare these results to our analysis as the Palm et al. [2020]  
 519 work chose to focus only on the total organic aerosol and total Abs 405 BrC and did not examine  
 520 the WSOC or water-soluble Abs 405. When examining the ratio of WSOC to  $\Delta\text{CO}$  as a function  
 521 of time since emission (Figure S5) during WE-CAN, there was not clear evidence for formation  
 522 or loss of WSOC being observed within a particular wildfire. But a recent analysis by Zeng et al.  
 523 [2022] has shown in wildfire plumes that dilution-drive evaporation was likely playing a minor  
 524 role compared to the effects of ozone on BrC.

525 In order to investigate the possible influence of fire dynamics on BrC absorption, the  
 526 modified combustion efficiency (MCE) was calculated as the change in carbon dioxide divided  
 527 by the sum of the change in carbon monoxide and carbon dioxide ( $\Delta\text{CO}_2/(\Delta\text{CO} + \Delta\text{CO}_2)$ ) on a  
 528 molar basis [Ward and Radke, 1993]. A higher MCE value indicates a more intense or extended  
 529 flaming phase as opposed to a smoldering phase. Within a particular wildfire there appeared to  
 530 be no clear dependence of the ratio of BrC absorption to WSOC,  $\Delta\text{CO}$ , or levoglucosan on MCE



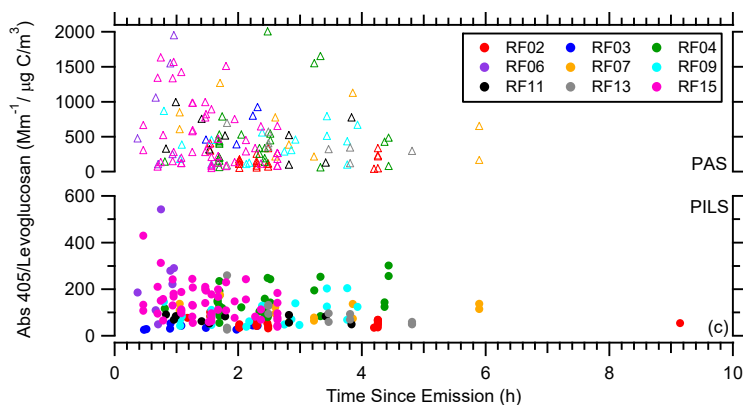


Figure 10. (a) Abs 405/WSOC, (b) Abs 405/ $\Delta$ CO, and (c) Abs 405/levoglucosan as a function of time since emission for all WE-CAN flights with the data segregated by flight. In each plot the PAS total Abs 405 BrC is on top and the PILS water-soluble Abs 405 on the bottom.

(Figure 11 and Figures S4-S6-S8), except that an overall lower Abs 405/levoglucosan ratio was observed for the wildfires with higher MCE values (i.e., Flight RF02). This further supports the relationship between the highest potassium concentrations and the levoglucosan vs. Abs 405 correlation (Figures 8e and 8d) previously discussed as potassium is predominately emitted from the flaming phase of a fire [Echalar *et al.*, 1995; Lee *et al.*, 2010; Ward *et al.*, 1991].

#### 4. Summary

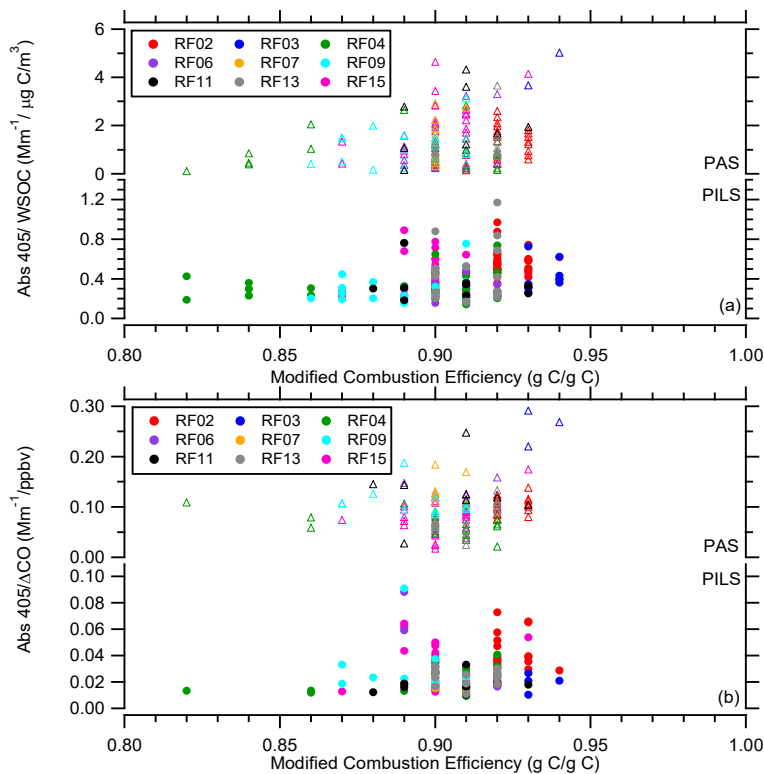
A PILS-LWCC-TOC and PAS were deployed on the NSF/NCAR C-130 research aircraft during WE-CAN to examine aerosol absorption in wildfire smoke in the western U.S. This was the first deployment of the PILS-LWCC-TOC on a research aircraft. The PILS allowed for a 16 s integrated measurement of the water-soluble BrC absorption and 4 s integrated measurement of WSOC. The data from the PILS and PAS were combined to investigate the water-soluble vs. total BrC absorption at 405 nm in the 20 wildfires sampled during WE-CAN. We show the following:

1. WSOC, PILS water-soluble Abs 405, and PAS total Abs 405 BrC tracked each other in and out of the smoke plumes. BrC absorption was correlated with CO ( $R^2$  value for PAS = 0.76 and PILS = 0.55) and WSOC ( $R^2$  value for PAS = 0.42 and PILS = 0.60) during the entire study, illustrating the importance of biomass burning as a source of BrC absorption. A similar pattern was observed for levoglucosan, but with two data branches. Levoglucosan and BrC absorption were correlated ( $R^2$  values for PAS = 0.60 and PILS = 0.76) in the first data branch and this subset of data was also characterized by the highest observed water-soluble potassium concentrations ( $> 0.5 \mu\text{g}/\text{m}^3$ ). This suggests there may be a relationship between levoglucosan and water-soluble potassium in wildfire emissions that has not generally been observed in other types of burning.
2. Using the calculated UHSAS mass, the PILS water-soluble Abs 405 can be corrected to also account for the non-water-soluble fraction of the aerosol. The corrected PILS water-

559 soluble Abs 405 showed good closure with the PAS total Abs 405 BrC, but with a factor  
 560 of ~1.5 to 2 difference. This difference can be explained by particle vs. bulk solution  
 561 absorption measured by the PAS vs. PILS, respectively, as shown by Mie Theory  
 562 calculations. During WE-CAN, ~45% of the BrC absorption at 405 nm was due to  
 563 water-soluble species.

564  
 565 3. The ratio of water-soluble ~~BrC absorption~~ Abs 405 to WSOC,  $\Delta$ CO, or levoglucosan  
 566 showed no clear dependence on fire dynamics or the time since emission up to 9 h. The  
 567 total Abs 405 BrC ~~absorption~~ did show a slight decrease in the first 2 h, suggesting a need  
 568 to further explore near source evolution.

569  
 570  
 571  
 572  
 573  
 574  
 575  
 576



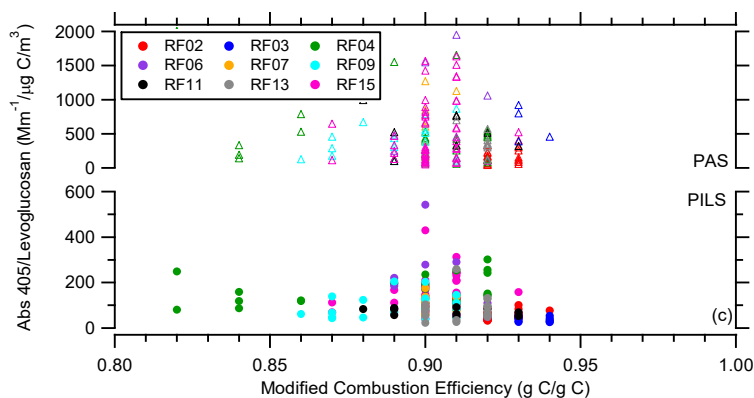


Figure 11. (a) Abs 405/WSOC, (b) Abs 405/ $\Delta$ CO, and (c) Abs 405/levoglucosan as a function of modified combustion efficiency for all WE-CAN flights with the data segregated by flight. In each plot the PAS total Abs 405 BrC is on top and the PILS water-soluble Abs 405 on the bottom.

577 **Data Availability**

578 The WE-CAN data is provided by NCAR/EOL under sponsorship of the National Science  
579 Foundation and is available at [http://data.eol.ucar.edu/master\\_lists/generated/we-can/](http://data.eol.ucar.edu/master_lists/generated/we-can/). The DOI  
580 for each data set used in this work are:

581  
582 PILS1: <https://doi.org/10.26023/9H07-MD9K-430D> and [https://doi.org/10.26023/CRHY-NDT9-](https://doi.org/10.26023/CRHY-NDT9-C30V)  
583 C30V

584 PILS2: <https://doi.org/10.26023/7TAN-TZMD-680Y>

585 PAS: <https://doi.org/10.26023/K8P0-X4T3-TN06>

586 UHSAS: <https://doi.org/10.26023/BZ4F-EAC4-290W>

587 CO: <https://doi.org/10.26023/NNYM-Z18J-PX0Q>

588 Meteorological Data and Coordinates: <https://doi.org/10.26023/G766-BS71-9V03>  
589

590 **Author Contributions**

591 APS, SMM, DWT, EVF, JLC designed the project. APS wrote the paper. APS, RPP, YS,  
592 SMM, DWT, TC, JL, and EVF collected and analyzed data. All authors reviewed and provided  
593 comments for the paper.  
594

595 **Conflict of Interest**

596 The authors declare that they have no conflict of interest.  
597

598 **Acknowledgements**

599 We wish to thank RAF personnel for their many contributions supporting the field deployment.  
600 We also thank R.J. Weber for generously providing some of the parts used in the PILS racks.  
601

602 **Financial Support**

603 This work was supported by the National Science Foundation under AGS-1650786.



604  
605  
606  
607  
608  
609  
610  
611  
612  
613  
614  
615  
616  
617  
618  
619  
620  
621  
622  
623  
624  
625  
626  
627  
628  
629  
630  
631  
632  
633  
634  
635  
636  
637  
638  
639  
640  
641  
642  
643  
644  
645  
646  
647  
648  
649  
650

**References**

Andreae, M.O. and A. Gelencsér, Black carbon or brown carbon? The nature of light-absorbing carbonaceous aerosols, *Atmos. Chem. Phys.*, *6*, 3131-3148, doi:10.5194/acp-6-3131-2006, 2006.

Arnott, W.P., H. Moosmüller, C.F. Rogers, T. Jin, and R. Bruch, Photoacoustic spectrometer for measuring light absorption by aerosol: instrument description, *Atmos. Environ.*, *33*, 2845-2852, 1999.

Chakrabarty, R.K., H. Moosmüller, L.-W. A. Chen, K. Lewis, W.P. Arnott, C. Mazzoleni, M.K. Dubey, C.E. Wold, W.M. Hao, and S.M. Kreidenweis, Brown carbon in tar balls from smoldering biomass combustion, *Atmos. Chem. Phys.*, *10*, 6363-6370, doi:10.5194/acp-10-6363-2010, 2010.

Craig, L., A. Moharreri, D. C. Rogers, B. Anderson, and S. Dhaniyala, Aircraft-Based Aerosol Sampling in Clouds: Performance Characterization of Flow-Restriction Aerosol Inlets, *Journal of Atmospheric and Oceanic Technology*, *31*, 2512-2521, doi:10.1175/jtech-d-14-00022.1, 2014.

Craig, L., A. Moharreri, A. Schanot, D. C. Rogers, B. Anderson, and S. Dhaniyala, Characterizations of Cloud Droplet Shatter Artifacts in Two Airborne Aerosol Inlets, *Aerosol Science and Technology*, *47*, 662-671, doi:10.1080/02786826.2013.780648, 2013a.

Craig, L., A. Schanot, A. Moharreri, D. C. Rogers, and S. Dhaniyala, Design and Sampling Characteristics of a New Airborne Aerosol Inlet for Aerosol Measurements in Clouds, *Journal of Atmospheric and Oceanic Technology*, *30*, 1123-1135, doi:10.1175/jtech-d-12-00168.1, 2013b.

651  
652 Desyaterik, Y., Y. Sun, X. Shen, T. Lee, X. Wang, T. Wang, and J.L. Collett Jr., Speciation of  
653 “brown” carbon in cloud water impacted by agricultural biomass burning in eastern  
654 China, *J. Geophys. Res.*, *118*, 7389-7399, doi:10.1022/jgrd.50561, 2013.  
655  
656 [Di Lorenzo, R.A., B.K. Place, T.C VandenBoer, and C.J. Young, Composition of Size-Resolved](#)  
657 [Aged Boreal Fire Aerosols: Brown Carbon, Biomass Burning Tracers, and Reduced](#)  
658 [Nitrogen, \*ACS Earth Space Chem.\*, \*2\*, 278-285, doi:10.1021/acsearthspacechem.7b00137,](#)  
659 [2018.](#)  
660  
661 [Di Lorenzo, R.A., R.A. Washenfelder, A.R. Attwood, H. Guo, L. Xu, N.L. Ng, R.J. Weber, K.](#)  
662 [Baumann, E. Edgerton, and C.J. Young, Molecular-Size-Separated Brown Carbon](#)  
663 [Absorption for Biomass-Burning Aerosol at Multiple Field Sites, \*Environ. Sci. Technol.\*,](#)  
664 [\*51\*, 3128-3137, doi:10.1021/acs.est.6b06160, 2017.](#)  
665  
666 Duarte, R.M.B.O., C.A. Pio, and A.C. Duarte, Spectroscopic study of the water-soluble organic  
667 matter isolated from atmospheric aerosols collected under different atmospheric  
668 conditions, *Analytica Chimica Acta*, *530*, 7-14, 2005.  
669  
670 Duarte, R.M.B.O., M. Piñeiro-Iglesias, P. López-Mahía, S. Muniategui-Lorenzo, J. Moreda-  
671 Piñeiro, A.M.S. Silva, and A.C. Duarte, Comparative study of atmospheric water-soluble  
672 organic aerosols composition in contrasting suburban environments in the Iberian  
673 Peninsula Coast, *Science of the Total Environment*, *648*, 430-441, 2019.  
674  
675 Eatough, D.J., A. Wadsworth, D.A. Eatough, J.W. Crawford, L.D. Hansen, and E.A. Lewis, A  
676 multiple system, multi-channel diffusion denuder sampler for the determination of fine-  
677 particulate organic material in the atmosphere, *Atmos. Environ.*, *27A*, 1213-1219, 1993.  
678  
679 Echalar, F., A. Gaudichet, H. Cachier, and P. Artaxo, Aerosol emissions by tropical forest and  
680 savanna biomass burning: Characteristic trace elements and fluxes, *Geophys. Res. Lett.*,  
681 *22*, 3039-3042, 1995.  
682  
683 Feng, Y., V. Ramanathan, and V.R. Kotamarthi, Brown carbon: a significant atmospheric  
684 absorber of solar radiation?, *Atmos. Chem. Phys.*, *13*, 8607-8621, doi:10.5194/acp-13-  
685 8607-2013, 2013.  
686  
687 Forrister, H., J. Liu, E. Scheuer, J. Dibb, L. Ziemba, K.L. Thornhill, B. Anderson, G. Diskin,  
688 A.E. Perring, J.P. Schwarz, P. Campuzano-Jost, D.A. Day, B.B. Palm, J.L. Jimenez, A.  
689 Nenes, and R.J. Weber, Evolution of brown carbon in wildfire plumes, *Geophys. Res.*  
690 *Lett.*, *42*, 4623-4630, doi:10.1002/2015GL063897, 2015.  
691  
692 Foster, K., R. Pokhrel, M. Burkhardt, and S. Murphy, A novel approach to calibrating a  
693 photoacoustic absorption spectrometer using polydisperse absorbing aerosol, *Atmos.*  
694 *Meas. Tech.*, *12*, 3351-3363, doi:10.5194/amt-12-3351-2019, 2019.  
695  
696 Gerbig, C., S. Schmitgen, D. Kley, A. Volz-Thomas, K. Dewey, and D. Haaks, An improved

697 fast-response vacuum-UV resonance fluorescence CO instrument, *J. Geophys. Res.*, *104*,  
698 1699-1704, 1999.

699

700 Hecobian, A., X. Zhang, M. Zheng, N.H. Frank, E.S. Edgerton, and R.J. Weber, Water-soluble  
701 organic aerosol material and the light-absorption characteristics of aqueous extracts  
702 measured over the Southeastern United States, *Atmos. Chem. Phys.*, *10*, 5965-5977,  
703 doi:10.5194/acp-10-5965-2010, 2010.

704

705 Hems, R.F. and J.P.D. Abbatt, Aqueous Phase Photo-oxidation of Brown Carbon Nitrophenols:  
706 Reaction Kinetics, Mechanism, and Evolution of Light Absorption, *ACS Earth Space*  
707 *Chem.*, *2*, 225-234, doi:10.1021/acsearthspacechem.7b00123, 2018.

708

709 Hoffer, A., A. Gelencsér, P. Guyon, G. Kiss, O. Schmid, G.P. Frank, P. Artaxo, and M.O.  
710 Andreae, Optical properties of humic-like substance (HULIS) in biomass-burning  
711 aerosols, *Atmos. Chem. Phys.*, *6*, 3563-3570, doi:10.5194/acp-6-3563-2006, 2006.

712

713 Jacobson, M.C., H.-C. Hansson, K.J. Noone, and R.J. Charlson, Organic atmospheric aerosols:  
714 Review and state of the science, *Rev. Geophys.*, *38*, 267-294, 2000.

715

716 Jo, D.S., R.J. Park, S. Lee, S.-W. Kim, and X. Zhang, A global simulation of brown carbon:  
717 implications for photochemistry and direct radiative effect, *Atmos. Chem. Phys.*, *16*,  
718 3413-3432, doi:10.5194/acp-16-3413-2016, 2016.

719

720 Kanakidou, M., et al., Organic aerosol and global climate modelling: a review, *Atmos. Chem.*  
721 *Phys.*, *5*, 1053-1123, doi:10.5194/acp-5-1053-2005, 2005.

722

723 Kirchstetter, T.W. and T.L. Thatcher, Contribution of organic carbon to wood smoke particulate  
724 matter absorption of solar radiation, *Atmos. Chem. Phys.*, *12*, 6067-6072,  
725 doi:10.5194/acp-12-6067-2012, 2012.

726

727 Kirchstetter, T.W., T. Novakov, and P.V. Hobbs, Evidence that the spectral dependence of light  
728 absorption by aerosols is affected by organic carbon, *J. Geophys. Res.*, *109*, D21208,  
729 doi:10.1029/2004JD004999, 2004.

730

731 Lack, D.A. and J.M. Langridge, On the attribution of black and brown carbon light absorption  
732 using the Ångström exponent, *Atmos. Chem. Phys.*, *13*, 10535-10543, doi:10.5194/acp-  
733 13-10535-2013, 2013.

734

735 Lack, D.A., J.M. Langridge, R. Bahreini, C.A. Brock, A.M. Middlebrook, and J.P. Schwarz,  
736 Brown Carbon and Internal Mixing in Biomass Burning Particles, *P. Natl. Acad. Sci.*,  
737 *109*, 14802-14807, doi:10.1073/pnas.1206575109, 2012.

738

739 Langridge, J.M., M.S. Richardson, D.A. Lack, C.A. Brock, and D.M. Murphy, Limitations of the  
740 Photoacoustic Technique for Aerosol Absorption Measurement at High Relative  
741 Humidity, *Aerosol Sci. Technol.*, *47*, 1163-1173, doi:10.1080/02786826.2013.827324,  
742 2013.

743  
744 Lee, T., A.P. Sullivan, L. Mack, J.L. Jimenez, S.M. Kreidenweis, T.B. Onasch, D.R. Worsnop,  
745 W. Malm, C.E. Wold, W.M. Hao, and J.L. Collett, Jr., Chemical smoke marker emissions  
746 during flaming and smoldering phases of laboratory open burning of wildland fuels,  
747 *Aerosol Res. Lett.*, *44*, i-v, 2010.  
748  
749 [Lee, A.K.Y., M.D. Willis, R.M. Healy, J.M. Wang, C.-H. Jeong, J.C. Wenger, G.J. Evans, and](#)  
750 [J.P.D. Abbatt, Single-particle characterization of biomass burning organic aerosol](#)  
751 [\(BBOA\): evidence for non-uniform mixing of high molecular weight organics and](#)  
752 [potassium, \*Atmos. Chem. Phys.\*, \*16\*, 5561–5572, doi:10.5194/acp-16-5561-2016, 2016.](#)  
753  
754 Limbeck, A., M. Kulmala, and H. Puxbaum, Secondary organic aerosol formation in the  
755 atmosphere via heterogeneous reaction of gaseous isoprene on acidic particles, *Geophys.*  
756 *Res. Lett.*, *30*(19), 1996, doi: 10.1029/2003GL017738, 2003.  
757  
758 Liu, J., M. Bergin, H. Guo, L. King, N. Kotra, E. Edgerton, and R.J. Weber, Size-resolved  
759 measurements of brown carbon in water and methanol extracts and estimates of their  
760 contribution to ambient fine-particle light absorption, *Atmos. Chem. Phys.*, *13*, 12389-  
761 12404, doi:10.5194/acp-13-12389-2013, 2013.  
762  
763 Liu, J., E. Scheuer, J. Dibb, G.S. Diskin, L.D. Ziemba, K.L. Thornhill, B.E. Anderson, A.  
764 Wisthaler, T. Mikoviny, J.J. Devi, M. Bergin, A.E. Perring, M.Z. Markovic, J.P.  
765 Schwarz, P. Campuzano-Jost, D.A. Day, J.L. Jimenez, and R.J. Weber, Brown carbon  
766 aerosol in the North American continental troposphere: sources, abundances, and  
767 radiative forcing, *Atmos. Chem. Phys.*, *15*, 7841-7858, doi:10.5194/acp-15-7841-2015,  
768 2015.  
769  
770 Liu, J., E. Scheuer, J. Dibb, L.D. Ziemba, K.L. Thornhill, B.E. Anderson, A. Wisthaler, T.  
771 Mikoviny, J.J. Devi, M. Bergin, and R.J. Weber, Brown carbon in the continental  
772 troposphere, *Geophys. Res. Lett.*, *41*, 2191-2195, doi:10.1002/2013GL058976, 2014.  
773  
774 Lukács, H., A. Gelencsér, S. Hammer, H. Puxbaum, C. Pio, M. Legrand, A. Kasper-Giebl, M.  
775 Handler, A. Limbeck, D. Simson, S. Preunkert, Seasonal trends and possible sources of  
776 brown carbon based on 2-year aerosol measurements at six sites in Europe, *J. Geophys.*  
777 *Res.*, *112*, D23S18, doi:10.1029/2006JD008151, 2007.  
778  
779 Marple, V.A., K.L. Rubow, and S.M. Behm, A microorifice uniform deposit impactor (MOUDI):  
780 description, calibration, and use, *Aerosol Sci. Technol.*, *14*, 434-446, 1991.  
781  
782 Moharreri, A., L. Craig, P. Dubey, D. C. Rogers, and S. Dhaniyala, Aircraft testing of the new  
783 Blunt-body Aerosol Sampler (BASE), *Atmospheric Measurement Techniques*, *7*, 3085-  
784 3093, doi:10.5194/amt-7-3085-2014, 2014.  
785  
786 Mohr, C., F.D. Lopez-Hilfiker, P. Zotter, A.S.H. Prévôt, L. Xu, N.L. Ng, S.C. Herndon, L.R.  
787 Williams, J.P. Franklin, M.S. Zahniser, D.R. Worsnop, W.B. Knighton, A.C. Aiken, K.J.  
788 Gorkowski, M.K. Dubey, J.D. Allan, and J.A. Thornton, Contribution of Nitrated Phenols

789 to Wood Burning Brown Carbon Light Absorption in Detling, United Kingdom during  
790 Winter Time, *Environ. Sci. Technol.*, 47, 6316-6324, 2013.

791

792 Moosmüller, H., R.K. Chakrabarty, W.P. Arnott, Aerosol light absorption and its measurement:  
793 A review, *J. Quant. Spectrosc. Radiat. Transfer*, 110, 844-878,  
794 doi:10.1016/j.jqsrt.2009.02.035, 2009.

795

796 Orsini, D.A., Y. Ma, A. Sullivan, B. Sierau, K. Baumann, and R.J. Weber, Refinements to the  
797 particle-into-liquid sampler (PILS) for ground and airborne measurements of water-  
798 soluble aerosol composition, *Atmos. Environ.*, 37, 1243-1259, 2003.

799

800 Palm, B.B., O. Peng, C.D. Fredrickson, B.H. Lee, L.A. Garofalo, M.A. Pothier, S.M.  
801 Kreidenweis, D.K. Farmer, R.P. Pöhrle, Y. Shen, S.M. Murphy, W. Permar, L. Hu, T.L.  
802 Campos, S.R. Hall, K. Ullmann, X. Zhang, F. Flocke, E.V. Fischer, and J.A. Thornton,  
803 Quantification of organic aerosol and brown carbon evolution in fresh wildfire plumes, *P.*  
804 *Natl. Acad. Sci.*, 117, 29469–29477, doi:10.1073/pnas.2012218117, 2020.

805

806 Pöhrle, R.P., E.R. Beamesderfer, N.L. Wagner, J.M. Langridge, D.A. Lack, T. Jayarathne, E.A.  
807 Stone, C.E. Stockwell, R.J. Yokelson, and S.M. Murphy, Relative importance of black  
808 carbon, brown carbon, and absorption enhancement from clear coatings in biomass  
809 burning emissions, *Atmos. Chem. Phys.*, 17, 5063-5078, doi:10.5194/acp-17-5063-2017,  
810 2017.

811

812 Saleh, R., C.J. Hennigan, G.R. McMeeking, W.K. Chuang, E.S. Robinson, H. Coe, N.M.  
813 Donahue, and A.L. Robinson, Absorptivity of brown carbon in fresh and photo-  
814 chemically aged biomass-burning emissions, *Atmos. Chem. Phys.*, 13, 7683-7693,  
815 doi:10.5194/acp-13-7683-2013, 2013.

816

817 Sareen, N., A.N. Schwier, E.L. Shapiro, D. Mitroo, and V.F. McNeill, Secondary organic  
818 material formed by methylglyoxal in aqueous aerosol mimics, *Atmos. Chem. Phys.*, 10,  
819 997-1016, doi:10.5194/acp-10-977-2010, 2010.

820

821 Saxena, P. and L.M. Hildemann, Water-soluble organics in atmospheric particles: A critical  
822 review of the literature and applications of thermodynamics to identify candidate  
823 compounds, *J. Atmos. Chem.*, 24, 57-109, 1996.

824

825 Schauer, J.J., M.J. Kleeman, G.R. Cass, and B.R.T. Simoneit, Measurement of Emissions from  
826 Air Pollution Sources. 3. C<sub>1</sub>-C<sub>29</sub> Organic Compounds from Fireplace Combustion of  
827 Wood, *Environ. Sci. Technol.*, 35, 1716-1728, 2001.

828

829 Simoneit, B.R.T., J.J. Schauer, C.G. Nolte, D.R. Oros, V.O. Elias, M.P. Fraser, W.F. Rogge, and  
830 G.R. Cass, Levoglucosan, a tracer for cellulose in biomass burning and atmospheric  
831 particles, *Atmos. Environ.*, 33, 173-182, 1999.

832

833 Sorooshian, A., F.J. Brechtel, Y. Ma, R.J. Weber, A. Corless, R.C. Flagan, and J.H. Seinfeld,  
834 Modeling and Characterization of a Particle-into-Liquid Sampler (PILS), *Aerosol Sci.*

835 *Technol.*, 40, 396-409, 2006.

836

837 Sullivan, A.P., H. Guo, J.C. Schroder, P. Campuzano-Jost, J.L. Jimenez, T. Campos, V. Shah, L.

838 Jaeglé, B.H. Lee, F.D. Lopez-Hilfiker, J.A. Thornton, S.S. Brown, and R.J. Weber,

839 Biomass Burning Markers and Residential Burning in the WINTER Aircraft Campaign,

840 *J. Geophys. Res.*, 124, doi:10.1029/2017JD028153, 2019.

841

842 Sullivan, A.P., N. Frank, D.M. Kenski, and J.L. Collett Jr., Application of High-Performance

843 Anion-Exchange Chromatography – Pulsed Amperometric Detection for Measuring

844 Carbohydrates in Routine Daily Filter Samples Collected by a National Network: 2.

845 Examination of Sugar Alcohols/Polyols, Sugars, and Anhydrosugars in the Upper

846 Midwest, *J. Geophys. Res.*, 116, D08303, doi:10.1029/2010JD014169, 2011b.

847

848 Sullivan, A.P., N. Frank, G. Onstad, C.D. Simpson, and J.L. Collett, Jr., Application of High-

849 Performance Anion-Exchange Chromatography – Pulsed Amperometric Detection for

850 Measuring Carbohydrates in Routine Daily Filter Samples Collected by a National

851 Network: 1. Determination of the Impact of Biomass Burning in the Upper Midwest, *J.*

852 *Geophys. Res.*, 116, D08302, doi:10.1029/2010JD014166, 2011a.

853

854 Sullivan, A.P., A.A. May, T. Lee, G.R. McMeeking, S.M. Kreidenweis, S.K. Akagi, R.J.

855 Yokelson, S.P. Urbanski, and J.L. Collett, Jr., Airborne-Based Source Smoke Marker

856 Ratios from Prescribed Burning, *Atmos. Chem. Phys.*, 14, 10535-10545, doi:10.5194/acp-

857 14-10535-2014, 2014.

858

859 Sumlin, B.J., A. Pandey, M.J. Walker, R.S. Pattison, B.J. Williams, and R.K. Chakrabarty,

860 Atmospheric Photooxidation Diminishes Light Absorption by Primary Brown Carbon

861 Aerosol from Biomass Burning, *Environ. Sci. Technol. Lett.*, 4, 540-545,

862 doi:10.1021/acs/estlett.7b00393, 2017.

863

864 Updyke, K.M., T.B. Nguyen, and S.A. Nizkorodov, Formation of brown carbon via reactions of

865 ammonia with secondary organic aerosols from biogenic and anthropogenic precursors,

866 *Atmos. Environ.*, 63, 22-31, 2012.

867

868 Verma, V., Y. Wang, R. El-Affifi, T. Fang, J. Rowland, A.G. Russell, and R.J. Weber,

869 Fractionating ambient humic-like substances (HULIS) for their reactive oxygen species

870 activity – Assessing the importance of quinones and atmospheric aging, *Atmos. Environ.*,

871 120, 351-359, 2015.

872

873 [Washenfelder, R.A., L. Azzarello, K. Ball, S.S. Brown, Z.C.J. Decker, A. Franchin, C.D.](#)

874 [Fredrickson, K. Hayden, C.D. Holmes, A.M. Middlebrook, B.B. Palm, R.B. Pierce, D.J.](#)

875 [Price, J.M. Roberts, M.A. Robinson, J.A. Thornton, C.C. Womack, and C.J. Young,](#)

876 [Complexity in the Evolution, Composition, and Spectroscopy of Brown Carbon in](#)

877 [Aircraft Measurements of Wildfire Plumes, \*Geophys. Res. Lett.\*, 49, e2022GL098951,](#)

878 [doi:10.1029/2022GL098951, 2022.](#)

879

880 Ward, D.E. and L.F. Radke, Emission measurements from vegetation fires: a comparative

881 evaluation of methods and results, in *Fire in the environment: the ecological,*  
882 *atmospheric, and climatic importance of vegetation fires*, edited by P.J. Crutzen and J.G.  
883 Goldammer, pp. 53-76, Wiley, Chichester, England, 1993.  
884

885 Ward, D.E., A.W. Setzer, Y.J. Kaufman, and R.A. Rasmussen, Characteristics of smoke  
886 emissions from biomass fires of the Amazon region-BASE-A experiment, in *Global*  
887 *Biomass Burning: Atmospheric, Climatic, and Biospheric Implications*, edited by J.S.  
888 Levine, pp. 394-402, MIT Press, Cambridge, MA, 1991.  
889

890 Wong, J.P.S., M. Tsagkaraki, I. Tsiodra, N. Mihalopoulos, K. Violaki, M. Kanakidou, J.  
891 Sciare, A. Nenes, and R.J. Weber, Atmospheric evolution of molecular-weight-  
892 separated brown carbon from biomass burning, *Atmos. Chem. Phys.*, *19*, 7319-7334,  
893 doi:10.5194/acp-19-7319-2019, 2019.  
894

895 Yttri, K.E., W. Aas, A. Bjerke, J.N. Cape, F. Cavalli, D. Ceburnis, C. Dye, L. Emblico, M.C.  
896 Facchini, C. Forster, J.E. Hanssen, H.C. Hansson, S.G. Jennings, W. Maenhaut, J.P.  
897 Putaud, and K. Tørseth, Elemental and organic carbon in PM10: a one year  
898 measurement campaign within the European Monitoring and Evaluation Programme  
899 EMEP, *Atmos. Chem. Phys.*, *7*, 5711-5725, 2007.  
900

901 Zeng, L., J. Dibb, E. Scheuer, J.M. Katich, J.P. Schwarz, I. Bourgeois, J. Peischl, T. Ryerson,  
902 C. Warneke, A.E. Perring, G.S. Diskin, J.P. DiGangi, J.B. Nowak, R.H. Moore, E.B.  
903 Wiggins, D. Pagonis, H. Guo, P. Campuzano-Jost, J.L. Jimenez, L. Xu, and R. J.  
904 Weber, Characteristics and Evolution of Brown Carbon in Western United States  
905 Wildfires, *Atmos. Chem. Phys. Discuss. [preprint]*, doi:10.5194/acp-2022-70, in  
906 review, 2022.  
907

908 Zeng, L., A. Zhang, Y. Wang, N.L. Wagner, J.M. Katich, J.P. Schwarz, G.P. Schill, C.  
909 Brock, K.D. Froyd, D.M. Murphy, C.J. Williamson, A. Kupac, E. Scheuer, J. Dibb,  
910 and R.J. Weber, Global Measurements of Brown Carbon and Estimated Direct  
911 Radiative Effects, *Geophys. Res. Lett.*, *47*, e2020GL088747,  
912 doi:10.1029/2020GL088747, 2020.  
913

914 Zhang, A., Y. Wang, Y. Zhang, R.J. Weber, Y. Song, Z. Ke, and Y. Zou, Modeling the  
915 global radiative effect of brown carbon: a potentially larger heating source in the  
916 tropical free troposphere than black carbon, *Atmos. Chem. Phys.*, *20*, 1901-1920,  
917 doi:10.5194/acp-20-1901-2020, 2020.  
918

919 Zhang, Q., et al., Ubiquity and dominance of oxygenated species in organic aerosols in  
920 anthropogenically-influenced Northern Hemisphere midlatitudes, *Geophys. Res. Lett.*,  
921 *34*, L13801, doi:10.1029/GL029979, 2007.  
922

923 Zhang, X., Y.-H. Lin, J.D. Surratt, and R.J. Weber, Sources, Composition and Absorption  
924 Ångström Exponent of Light-absorbing Organic Components in Aerosol Extracts  
925 from the Los Angeles Basin, *Environ. Sci. Technol.*, *47*, 3685-3693,  
926 doi:10.1021/es305047b, 2013.

927  
928 Zhang, X., Y.-H. Lin, J.D. Surratt, P. Zotter, A.S.H. Prévôt, and R.J. Weber, Light-absorbing  
929 soluble organic aerosol in Los Angeles and Atlanta: A contrast in secondary organic  
930 aerosol, *Geophys. Res. Lett.*, *38*, L21810, doi:10.1029/2011GL049385, 2011.  
931  
932 Zhang, Y., H. Forrister, J. Liu, J. Dibb, B. Anderson, J.P. Schwarz, A.E. Perring, J.L.  
933 Jimenez, P. Campuzano-Jost, Y. Wang, A. Nenes, and R.J. Weber, Top-of-  
934 atmosphere radiative forcing affected by brown carbon in the upper troposphere,  
935 *Nature Geoscience*, *10*, 486-489, doi:10.1038/NGEO2960, 2017.  
936  
937 Zhao, R., A.K.Y. Lee, L. Huang, X. Li., F. Yang, and J.P.D. Abbatt, Photochemical  
938 processing of aqueous atmospheric brown carbon, *Atmos. Chem. Phys.*, *15*, 6087-  
939 6100, doi:10.5194/acp-15-6087-2015, 2015.  
940  
941 Zhong, M. and M. Jang, Dynamic light absorption of biomass-burning organic carbon  
942 photochemically aged under natural sunlight, *Atmos. Chem. Phys.*, *14*, 1517-1525,  
943 doi:10.5194/acp-14-1517-2014, 2014.  
944